Journal of Materials Chemistry B

PAPER

View Article Online
View Journal | View Issue

Cite this: J. Mater. Chem. B, 2015, 3, 5070

Supplementing π-systems: eumelanin and graphene-like integration towards highly conductive materials for the mammalian cell culture bio-interface†

Valentina Gargiulo,[a] Michela Alfè,[a] Roberto Di Capua,[bc] Anna Rita Togna,[d] Vittoria Cammisotto,[d] Silvana Fiorito,[ef] Anna Musto,[gh] Angelica Navarra,[gh] Silvia Parisi[gh] and Alessandro Pezzella*[ij]

Received 17th February 2015,
Accepted 9th April 2015

DOI: 10.1039/c5tb00343a

www.rsc.org/MaterialsB

Organic (bio)electronics appears to be the first target for competitive exploitation in the materials science of eumelanins, black insoluble photoprotective human biopolymers. Nonetheless, the low conductivity of these pigments is limiting the implementation of eumelanin-based devices. Here we present a novel organic/organic hybrid material (EUGL) by integration of conductive graphene-like (GL) layers within the EUmelanin pigment (EU). GL layers were obtained by a two-step oxidation/reduction of carbon black. The stability of GL layers over a wide pH range and the self-assembling tendency place this material in a leading position for the fabrication of hybrid materials in aqueous media. EUGL was obtained by inducing the polymerization of eumelanin precursors (5,6-dihydroxyindole, DHI and 5,6-dihydroxyindole-2 carboxylic acid, DHICA) in aqueous media containing GL layers. The new material featured promising biocompatibility and an increased conductivity with respect to eumelanin by four orders of magnitude.

Introduction

The scope of organic (bio)electronics[1,2] is largely dictated by the chemical nature of the materials that transduce signals across the biotic/abiotic interface. Among materials under investigation as candidates for functional biocompatible interfaces, the human pigment eumelanin is currently gaining increasing interest.[3–6] This black insoluble and heterogeneous pigment of human skin, hair, eyes and nigral neurons (neuromelanin)[7,8] arises biogenetically from the amino acid tyrosine *via* the oxidative polymerization of 5,6-dihydroxyindole (DHI) and/or 5,6-dihydroxyindole-2-carboxylic acid (DHICA).[5] A distinctive trait of eumelanin(s) is its unique assortment of chemical–physical properties[3] including: (a) broadband optical absorption in the UV-visible range;[9,10] (b) efficient UV-dissipative mechanisms;[11] (c) photoconductivity in the solid state;[12] (d) electronic–ionic hybrid conducting properties;[13,14] (e) hydration-dependent free radical properties;[15] and (f) metal ion-binding properties.[16]

From the structural point of view eumelanins appear as complicated disordered mixtures of different oligomeric and polymeric species arising by oxidative polymerization of the two indoles DHI and DHICA.[5] Nonetheless, a series of studies[5] have proved that DHI–eumelanin[5] prepared by the oxidation of indole under biomimetic conditions can efficiently act as a model of the natural pigment.[17] Key elements characterizing DHI polymerization and the resultant eumelanin can be summarized as follows: (a) DHI polymers grow mainly *via* monomer–polymer or low oligomer–polymer coupling steps, rather than by large oligomer–oligomer interactions and the maximum apparent size of the aggregates attainable before precipitation is *ca.* 1200 nm;[18] (b) the visible chromophore development associated with polymer growth reflects a dual component, an intrinsic one, and an extrinsic dynamic one;[9,10] and (c) the fundamental aggregates look like 2D planar sheets[18] (Fig. 1).

Both chemical–physical properties and structural features are the basis of interest toward this pigment,[4] however two main

[a] Istituto di Ricerche sulla Combustione (IRC) – CNR, P.leTecchio 80, I-80125 Naples, Italy
[b] Dipartimento di Fisica, Università di Napoli Federico II via Cintia, I-80126, Naples, Italy
[c] CNR-SPIN via Cintia, Naples I-80126, Italy
[d] Department of Physiology and Pharmacology "Vittorio Erspamer", Sapienza University of Rome, P.le A. Moro 5, 00185 Rome, Italy
[e] Department of Clinical Medicine, Sapienza University of Rome, P.le A. Moro 5, 00185 Rome, Italy
[f] Inst. of Translational Pharmacology, National Research Council (CNR), Rome, Italy
[g] Department of Molecular Medicine and Medical Biotechnology, University of Naples "Federico II", Naples, Via Pansini, 5- 80131- Napoli, Italy
[h] Ceinge Biotecnologie Avanzate Via Gaetano Salvatore 486, 80145 Naples, Italy
[i] Department of Chemical Sciences, University of Naples "Federico II" Via Cintia 4, I-80126 Naples, Italy. E-mail: alessandro.pezzella@unina.it
[j] Institute for Polymers, Composites and Biomaterials (IPCB), CNR, Via Campi Flegrei 34, 80078 Pozzuoli (Na), Italy

† Electronic supplementary information (ESI) available. See DOI: 10.1039/c5tb00343a

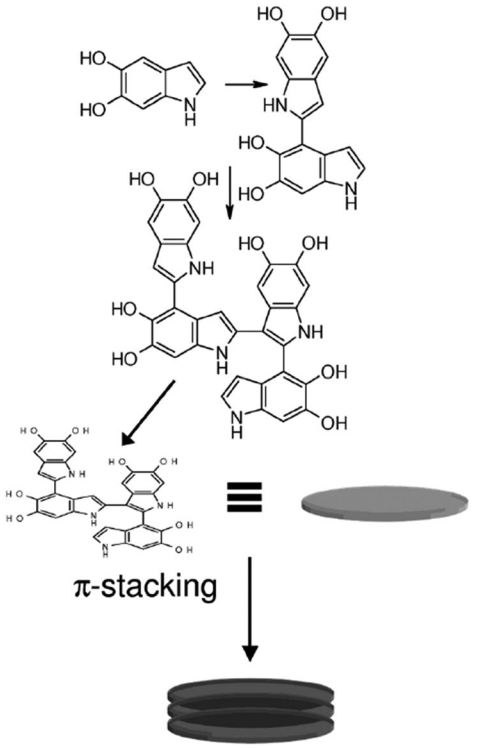

Fig. 1 Schematic outline of eumelanin buildup.

obstacles hampered the full exploitation of eumelanin based devices: (a) the actual insolubility of eumelanin in any solvent,[3] preventing easy processability of the pigment as well as device fabrication; and (b) its low conductivity,[15] limiting both the range of possible working potential and functional applications.

On the other hand, eumelanin biocompatibility[19–21] makes this material a leading candidate of choice in a series of applications including: (a) functional interfaces connecting biological systems to electrical devices,[4,22] (b) devices translating optical and electronic stimuli into biosignals for engineering functional biological tissues,[23] (c) devices for advanced cell culture systems and single-cell managing,[24] and (d) devices for cell sorting and differentiation.[25]

In this scenario, a number of studies have recently reported eumelanin based functional devices[14,26,27] as well as eumelanin films for nerve tissue engineering[23] and nonwoven fibers for cardiac tissue engineering.[19]

In a systematic investigation some of us addressed the issue of eumelanin processability focusing on thin film fabrication with the main goal of obtaining both a complete chemical-structural control of the material and high quality film morphology. The combined use of biomimetic DHI oxidative polymerization and soft deposition techniques such as MAPLE (Matrix Assisted Pulsed Laser Evaporation) allowed us to achieve the first objective[28,29] while the design and development of the *ad hoc* solid state protocol for DHI oxidative polymerization (Ammonia Induced Solid State Polymerization, AISSP) allowed us to obtain high quality, easily accessible biocompatible eumelanin thin films.[30]

Although eumelanin films obtained using the AISSP protocol did show water dependent charge transport properties,[14,30] the electrical properties of these films still are far from the standards required in organic (bio)electronics.

Among the different strategies under investigation to improve electrical performance of eumelanin thin films, a clear-cut approach lies in hybridization with a suitable conductive counterpart.

Delocalized electrons of π-conjugated molecules offer a conductive pathway along their skeleton, attracting great interest in the production of organic nanodevices.[31,32] Numerous reports addressing the use of carbon nanotubes, reduced graphite oxide, graphene and graphene-like thin films as ideal transparent electrodes for optoelectronic devices have been presented in the past few years.[33–35]

In this frame, some of us recently developed a high yield and environmentally advantageous protocol for the fabrication of conductive graphene-like (GL, Fig. 2) layers through a two-step oxidation/reduction method, starting from nanostructured carbon black (CB).[36] Thanks to the residual oxygen functional groups on the graphene layer edges, GL layers feature good stability in water resulting in a very versatile nanomaterial and the first candidate for the preparation of hybrid materials.[37]

Here we present the first (to the best of our knowledge) preparation of a eumelanin/GL layers hybrid material (EUmelanin-Graphene-Like, EUGL) featuring valuable functional and processing

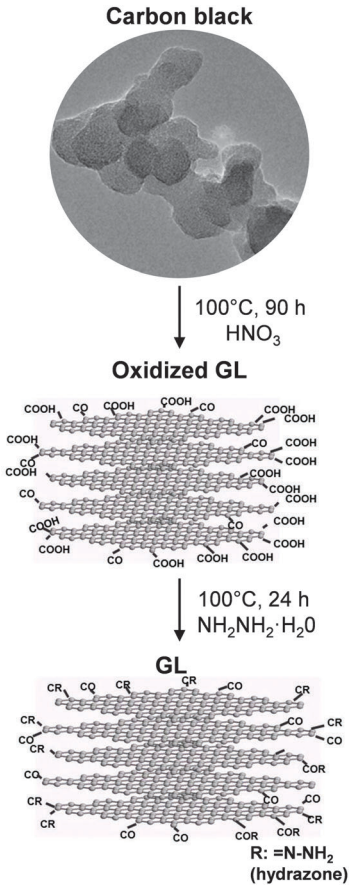

Fig. 2 Synthetic pathway and representation of the hypothesized morphologies of GL layers.

properties, including biocompatibility, easy filmability, high adhesion, and electrical conductivity.

The hybrid was characterized by chemical, physical, electrical and morphological analyses and its biocompatibility and toxicity were investigated in view of its potential exploitation as a bio-interface.

Results and discussion

Chemical–physical characterization

EUGL was characterized by integrating analytical and instrumental techniques. The elemental composition (C, N, and H) of EUGL together with those of pure eumelanin and GL layers is reported in Table 1. The oxygen amount was evaluated by difference. GL layers exhibit a significant amount of oxygen (39.6 wt%) indicating the presence of oxygen functional groups. The presence of nitrogen is also observed (6.09 wt%). The COOH amount, evaluated by a fluorimetric test,[38] is 1.6×10^{-7} mol_{COOH} mg^{-1}. The O/C element ratio is 0.56 (comparable to the graphene layers obtained from the reduction of graphite oxide by hydrazine[39]).

The measured values of C, H and N in the hybrid were compared with a linear combination (1/1 ratio) of measured values for GL layers and eumelanin (see Table 1, brackets). The comparison featured a fair accordance of data, suggesting the actual composition of the hybrid as the outcome of almost quantitative merging of the starting materials associated with some oxygen defects likely due to the loss of carboxylic groups.[40]

The comparison of infrared spectroscopy data showed the coexistence of the typical signature of both eumelanin and GL layers in the EUGL spectrum (Fig. 3) indicating the successful merging of the two starting materials. Moreover a comparison with the spectrum of the starting mixture of indoles confirms the actual formation of eumelanin in the presence of GL layers. The broadband feature of the EUGL spectrum is indicative of the π-domain growth, also evidenced by the higher absorption in the visible region, with respect to pure eumelanin (Fig. S1a and b in ESI†).

The main characteristic features of the infrared spectrum of GL layers are a broad band in the 3000–3700 cm^{-1} range (O–H stretching vibrations due to carboxylic and phenolic groups and possibly adsorbed H_2O and, at lower wavenumbers, the N–H stretching band due to NH_2 functionalities likely in the form of hydrazones), bands at 1650–1750 cm^{-1} (C═O stretching vibrations from carbonyl and carboxyl groups, anhydrides, lactones, single ketones and quinones) and bands at 1500–1600 cm^{-1} (skeletal vibration of the π-conjugated graphitic domains). Nitrogen atoms in the form of nitro groups were also detected (typical $-NO_2$ stretching vibration bands at 1560 and 1350 cm^{-1}).

Table 1 Composition of samples

		Elemental composition wt%			
Sample	GL wt%	C	O	H	N
Eumelanin	0	48.5	36.2	4.0	11.3
GL layers	100	52.9	39.6	1.4	6.1
EUGL	50	54.4 (50.7)	32.3 (37.9)	3.9 (2.7)	9.4 (8.7)

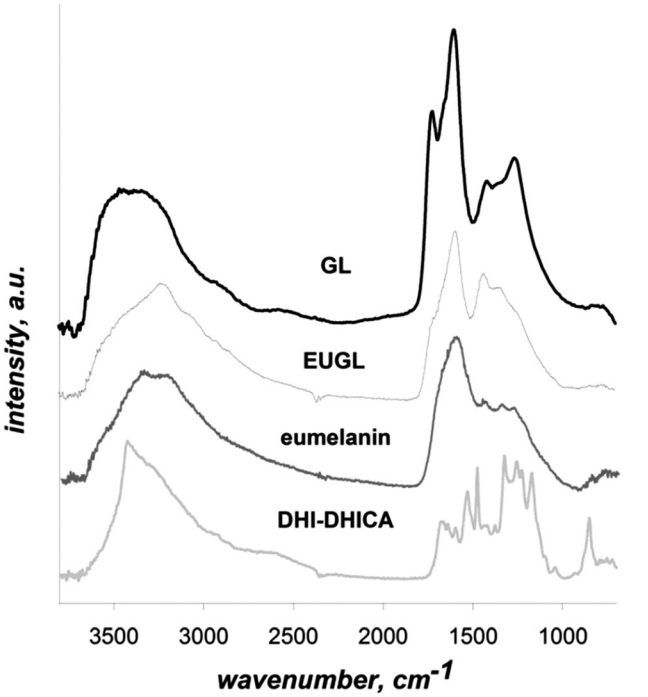

Fig. 3 ATR-IR spectra of the parent materials and the hybrid in the 3700–700 cm^{-1} wavenumber region. Spectra are baseline corrected and shifted.

EUGL was also investigated by thermogravimetric analysis (TGA) measuring the mass loss of the samples upon heating from room temperature up to 800 °C in an oxidative environment (Fig. 4).

The TGA curve of GL layers exhibits one main sharp weight loss at 550 °C, corresponding to the bulk oxidation of the GL graphitic core. In the case of the TGA curve of both eumelanin and eumelanin precursors a gradual weight loss between 150 and 600 °C is observed, which was likely due to the decomposition of labile oxygen bearing functional groups. A characteristic more pronounced weight loss at 200 °C (20% weight loss) is also observable for eumelanin. The thermal profile of EUGL exhibits features similar to those of parent materials (weight loss at 200 °C and 550 °C, the latter corresponding also to the EUGL burnoff). Furthermore, the absence of a sharp weight drop at around 550 °C, observed in the case of neat GL layers, suggests intimate contact between the components of the hybrid (eumelanin and GL layers). Although it is not possible to produce conclusive hypothesis for the eumelanin–GL layer interaction, both covalent bonds and π–π stacking are expected to be involved. Covalent bonds may arise following the attack of nucleophilic units of the GL layers (residual OH and NH_2 groups)[36] toward electrophilic moieties of eumelanin precursors, chiefly quinone and quinonoid systems. π–π stacking is expected based on the known tendency of graphene related materials to interact with aromatic systems.[41,42]

A comparative atomic force microscopy (AFM) inspection of the morphology of eumelanin, GL layers and EUGL thin films indicates a serious modification induced by eumelanin to the self-assembly of GL layers and associated adhesion behavior.

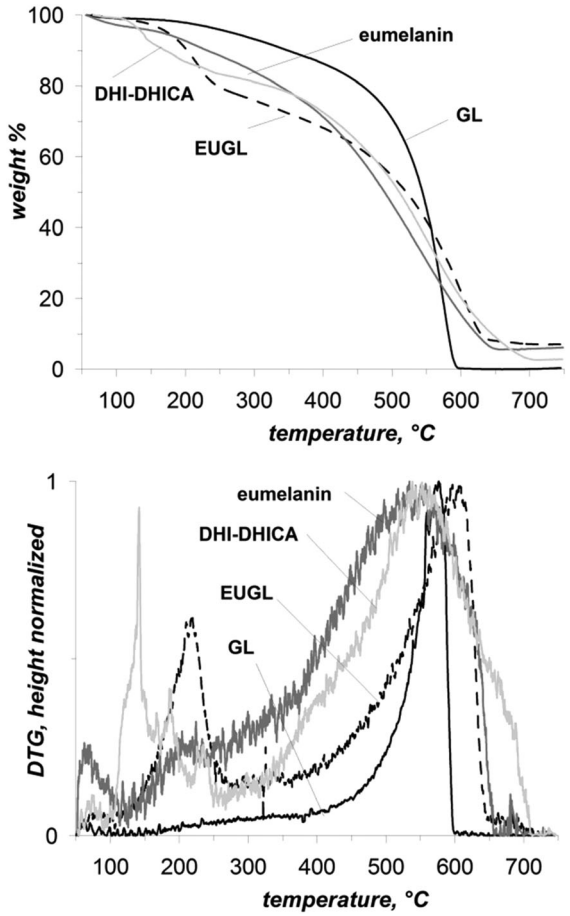

Fig. 4 Thermal analyses (TGA and DTG) of the parent materials and the hybrid in an oxidative environment (air).

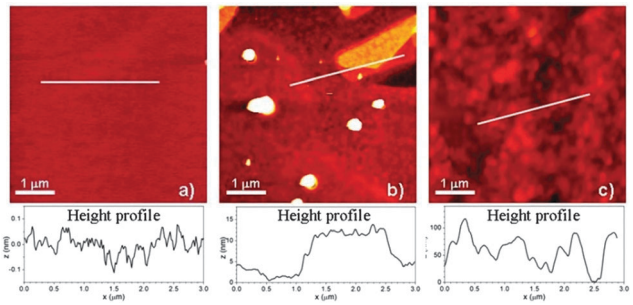

Fig. 5 AFM: non-contact AFM images, 5 μm × 5 μm, on: (a) GL layers; (b) eumelanin; (c) EUGL. On each image, a height profile on a line of about 3 μm is also reported, to highlight the surface roughness of each sample. For more detailed images see the ESI,† Fig. S2.

Indeed, the surface of the neat GL film in Fig. 5a appears to be atomically flat over large areas, with a root mean square (rms) roughness of below 1 Å. In contrast, eumelanin and EUGL surfaces exhibit a higher roughness, with different general features. Besides the local roughness, the eumelanin surface (Fig. 5b) appears to be made of larger regions and terraces, sharply delimited and exhibiting different morphologies: the height profile taken along the white line in Fig. 5b shows that such surface regions have heights ranging from a few to about 10 nm. The hybrid has a locally more granular surface (Fig. 5c), resulting in a higher rms roughness compared to eumelanin (about 32 nm *vs.* 10 nm); however, the general aspect is much more homogenous, exhibiting the same granular aspect over all the samples without sharply defined inhomogeneous regions. It must also be pointed out that the granular feature increases the effective exposed surface by about 15% compared to its "nominal" area.

Electrical properties

Electrical characterization also confirms the actual alteration between the properties of EUGL and its parent materials. The measurements of electrical dc resistivity (Fig. 6) have been carried out in a standard four contact geometry for the resistivity evaluation. In Fig. 6a–c, current *vs.* voltage curves for all the three samples are reported. All the curves show an ohmic behavior, but with an extremely different resistance: such strictly linear *I–V* behavior has already been observed for eumelanin pigments at a wide range of voltages,[43] although some deviations from ohmic behavior were reported at high voltages[44] (nonohmic *I–V* characteristics and Child's power law at high enough voltage can be a signature of ion transport[45]). A reliable comparison between samples of known thickness is given by the electrical resistivity ρ (or, equivalently, conductivity $\sigma = 1/\rho$), which can be calculated from measuring the resistance of the adopted geometry through the van der Pauw algorithm.[46] The thickness measurements have been performed through the AFM: the eumelanin sample was about 100 nm thick, while the GL layers and hybrid films were a few microns thick (4 μm and 3 μm respectively). The following resistivity values were estimated:

GL: $\rho_{GL} = (40 \pm 5)\ \Omega$ cm ($\sigma_{GL} = (2.5 \pm 0.3) \times 10^3$ S cm^{-1});

eumelanin: $\rho_{EU} = (2.8 \pm 0.4) \times 10^7\ \Omega$ cm
($\sigma_{EU} = (3.6 \pm 0.5) \times 10^{-8}$ S cm^{-1});

EUGL: $\rho_{EUGL} = (1.1 \pm 0.2) \times 10^3\ \Omega$ cm
($\sigma_{EUGL} = (9 \pm 2) \times 10^{-4}$ S cm^{-1}).

The high and poor electrical conductivity of GL layers and eumelanin, respectively, is not surprising. In particular, the estimated eumelanin conductivity lies in the middle of the wide range of measured values for eumelanin samples[15,36] (eight orders of magnitude, since electrical transport in eumelanin is strongly affected by some extrinsic factors such as humidity or photodoping).

On the other hand EUGL exhibits an electrical conductivity more than four orders of magnitude greater than parent eumelanin. Another interesting finding is the observation of time-decay of electrical conductivity in eumelanin and hybrid samples (while this phenomenon is absent in the GL film). As shown in Fig. 6d, the decay of σ takes place, on the two samples, on very different time scales and in very different amounts, being much faster and pronounced in eumelanin than in the hybrid compound. On the other hand, a common feature is the presence of two different time-scales in the decay curves: both curves exhibit a

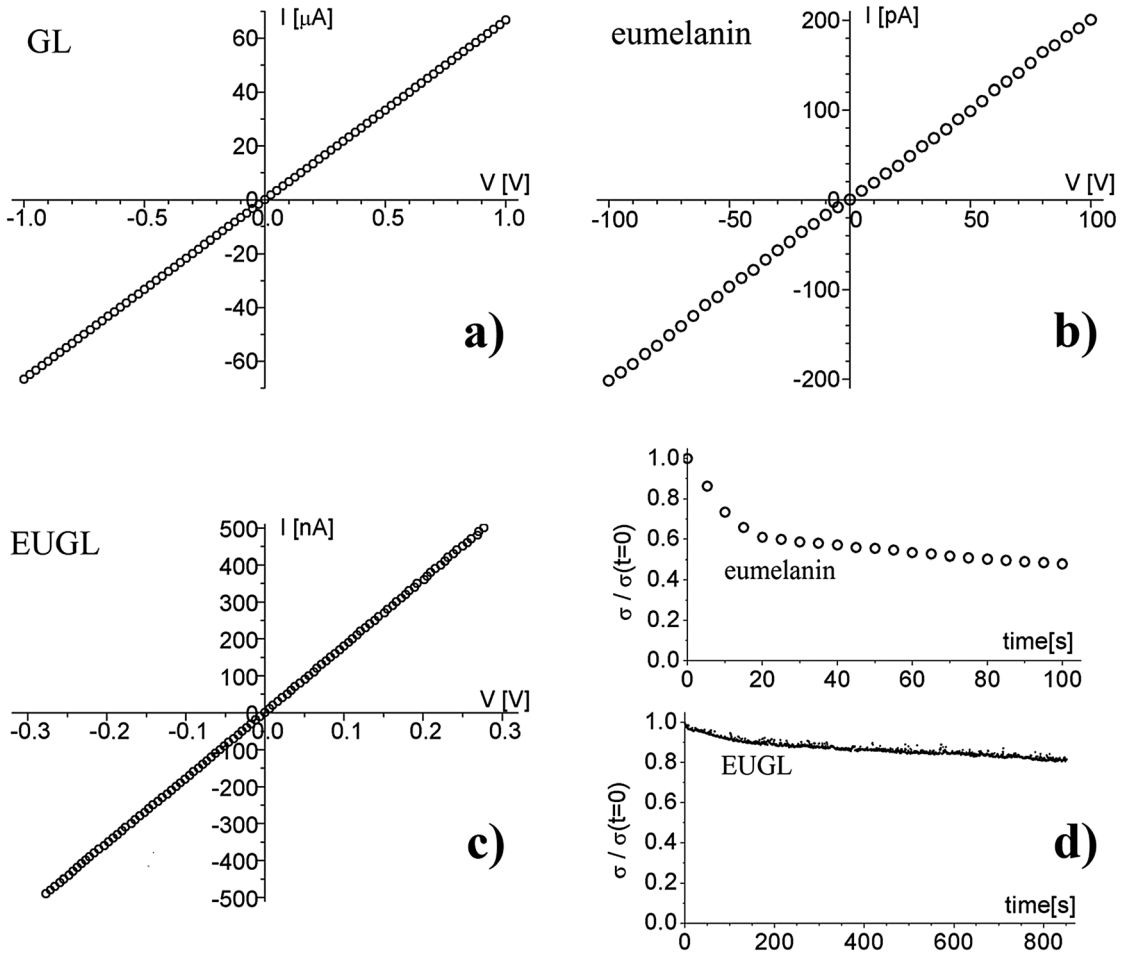

Fig. 6 *I–V* curves (in one of the two directions of the van der Pauw configuration) acquired on (a) GL layers, (b) eumelanin, and (c) EUGL samples. (d) Time-dependent decay of the electrical conductivity on the eumelanin and EUGL films, at a fixed voltage (100 V for the eumelanin, 100 mV for the hybrid).

"fast" initial decay, followed by a further slower decrease. The transition between the two regimes takes place after less than 20 s (and at about 60% of the initial conductivity) in eumelanin, and after a time about 10 times larger (at about 90% of its initial conductivity) in the hybrid material.

This result is in qualitative agreement with what recently observed for similar eumelanin samples[14] and somehow similar to the results reported on other (eu)melanin samples.[47] The fast initial decay can be probably ascribed to the ionic current that can flow in eumelanin or in the hybrid, but it is blocked at the silver electrodes designed for the measurements. More precisely, weakly bonded protons (H^+) in the interspaces of the stacked structure of our compounds can be driven by the applied electric field, producing the ionic current in the measured samples. However, such current flow cannot take place in the conventional metal constituting the electrodes, and protons are therefore blocked at the interface between the samples and the electrodes. The resulting counter-field is responsible for the observed initial decay of the electrical conductivity *vs.* time. After this transient, only the electronic contribution survives, but it also experiences a slower time decay, which is probably driven by trapping phenomena occurring in such disordered samples. Therefore, the σ decay and its double time-scale suggest the presence of a double contribution (ionic and electronic) to the electrical transport in both eumelanin and hybrid samples. On the contrary, in the GL film we did not observe any decrease of the electrical conductivity *vs.* time: this does not necessarily mean that proton transport does not occur, but, if it occurs, it is completely overruled by electron conductivity. The stronger incidence of the initial fast decay in eumelanin seems to indicate that in this sample the ionic contribution is much more important (relatively to the electronic one) than in the hybrid compound: in the latter, therefore, the conjunction with the GL layers adds electronic carriers that are likely responsible for the improved electrical conductivity.

Impedance spectroscopy measurements between 10 Hz and 100 kHz are reported in Fig. 7a–c, for the GL layers, eumelanin and EUGL samples, respectively. In this frequency range, the experimental data are well fitted by a common equivalent Randless circuit, schematically reported in Fig. 7d. In this model, CPE is a constant phase element, whose complex impedance *vs.* angular frequency ω can be written as $Z_{CPE} = 1/(j\omega)^m Q$: j is the imaginary unit, Q and m (with $0 \leq m \leq 1$) are fitting parameters (for $m = 0$ the CPE acts as a pure resistor of value Q^{-1}; for $m = 1$, it acts as a

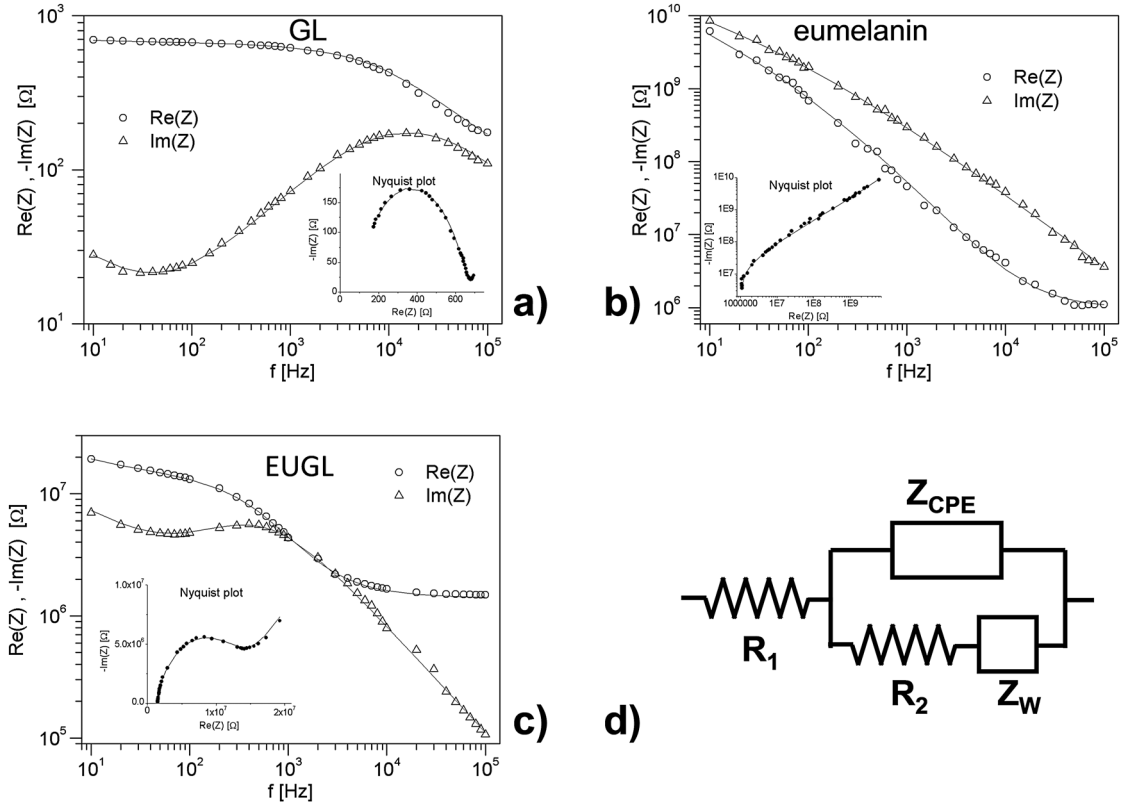

Fig. 7 Impedance spectroscopy measurements on (a) GL layers, (b) eumelanin, and (c) EUGL, plotted as real and imaginary part *vs.* frequency. In the insets: Nyquist plot per each set of measurements. Each plot reports both experimental data (scatter) and the theoretical fit (continuous line). (d) The Randless circuit is used for modeling the experimental impedance curves.

pure capacitor Q). Z_W is the impedance of a Warburg element: $Z_W = A_W/(j\omega)^{1/2}$. The Randless scheme is phenomenologically introduced to describe the ac transport in many complex organic compounds: Z_{CPE} includes the effects of a double layer capacitance and a surface modification capacitance, while the Warburg element describes the diffusion to the electrode surface. In our case, the use of the Randless circuit is suggested by the data on EUGL, whose Nyquist plot (inset of Fig. 7c) exhibits the typical features produced by this model: a ''smashed'' semi-circle as a consequence of the non-ideal capacitance of the CPE, and an upward nearly-linear arm due to the role of the Warburg element at low frequencies. It is worth noting, from Fig. 7b (and its inset), that the data on eumelanin do not show these strong signs: we decided however not to change the fitting model to avoid further introduction of degrees of freedom and to allow a direct comparison between the results on both samples. The fit procedure gives for the eumelanin sample $m = 0.99$: the CPE basically acts as a pure capacitor. We estimate a specific capacitance of about 1 μF cm^{-2}, which, however, is likely an underestimation of the intrinsic specific capacitance of the material (due to the poor grain connection). As a comparison, we get $m = 0.88$ on EUGL, and a pronounced role of the Warburg impedance already in the explored frequency range (on eumelanin, the fit curve is quite non-sensitive to the Warburg arm of the circuit: lower frequencies need to be explored to understand the role of this element). This difference can be an indication of relevant forward–backward jumps of the ions in the ac transport;[48] however, this result could also be a consequence of the worst connection between the different large regions of the eumelanin films than between the grains in the EUGL hybrid sample. As concerns the GL layers, the Randless circuit must also be invoked to get a satisfying fit, as already observed for reduced graphene oxide.[49]

Mammalian cell biocompatibility

Biocompatibility of EUGL was checked in mammalian cell cultures *in vitro*. In order to screen a range of different cellular requirements two different cell typologies were chosen: the Murine Embryonic Stem Cell (ESC) and Rat Microglial Cell (MC). ESC is a cell population of particular interest for tissue engineering application and it is under scrutiny for compatibility with classical electro-active materials.[50] The MCs are a cell population belonging to the class of neuroglial cells that play an active role in the central nervous system (CNS) function/homeostasis and are highly sensitive to electrical stimuli. They are the primary cells that are activated in response to inflammatory stimulation[51] and thus they are of particular relevance in the investigation of the toxic/proinflammatory potential of an electroconductive substrate.

Few previous papers have appeared in this field, one reporting the ability of thin films from commercial eumelanin to enhance Schwann cell growth and neurite extension film growth,[23] and a study on these specific ESCs disclosing the biocompatibility of AISSP fabricated eumelanin thin film.[30]

In a series of experiments we addressed the survival and proliferation of undifferentiated ESCs grown on EUGL films and the preservation of ESC morphology. Before cell seeding EUGL film stability to culture media was checked. Even after extensive sonication treatment in buffer the films remained stable and no detectable release of GL layers as well as eumelanin was observed.

To assess the ability of EUGL films to support the survival of ESCs, undifferentiated ESCs were trypsinized into a single-cell suspension and 6×10^4 cells per cm^2 were plated on 100 mm EUGL-coated dish in ESC medium. The medium was changed every day for two days. As shown in Fig. 8 EUGL coating supported adhesion and colony formation of ESCs. ESC proliferation was evaluated by counting cells after trypsinization and dissociation at 2 days in colonies plated on dishes coated with EUGL or with gelatin (as control).

As reported in Fig. S3 of the ESI† the growth curve of ESCs plated on EUGL showed a trend comparable with the same cells plated on gelatin, indicating that EUGL supports ESC proliferation.

In a separate experiment the level of the apoptosis hallmark active caspase-3 was analyzed in order to check the absence of abnormal cell death in healthy colonies and highlighted by the morphological analysis. As shown in Fig. S4 of ESI,† western blot analysis revealed that there is no accumulation of cleaved caspase-3 to the detriment of the uncleaved one that is normally present in healthy cells.

The *in vitro* viability of MC cultures over EUGL films was tested by different approaches: checking the release from damaged cells of the cytosolic enzyme lactate dehydrogenase (LDH)[52] by using a LDH diagnostic kit; and the possible effect on the cell mitochondrial function by the MTT test [3-(4,5-dimethylthiazol-2-yl)-2,5-diphenyltetrazolium bromide (MTT)].[53]

The measurement of LDH in the cell culture supernatants after 24 h indicated no significant increase of LDH levels in supernatants of cells grown on EUGL, indicative of a negligible cytotoxicity of these substrates on microglia cells. Interestingly, the levels of LDH in cell culture supernatants of cells grown on eumelanin substrates were significantly increased (Fig. 9) showing a cytotoxic potential of this substrate towards microglial cells. The MTT test further confirmed microglial cell viability over EUGL.

In a further series of experiments the analysis of NO production by microglia cells seeded on EUGL was addressed showing that no inflammatory potential could be ascribed to the EUGL substrate confirming the actual MC viability when cultured *in vitro* over the EUGL substrate (Fig. S5 of ESI†).

Overall, these data disclose the wide biocompatibility of EUGL being not toxic to ESCs and MCs and bereft of pro-inflammatory potential towards microglial cells. It is interesting to observe here that, differently from EUGL films, eumelanin films do not only affect significantly the viability of microglial cells but possess a remarkable pro-inflammatory potential towards these cells. This could be due to the phagocytic nature of microglial cells,

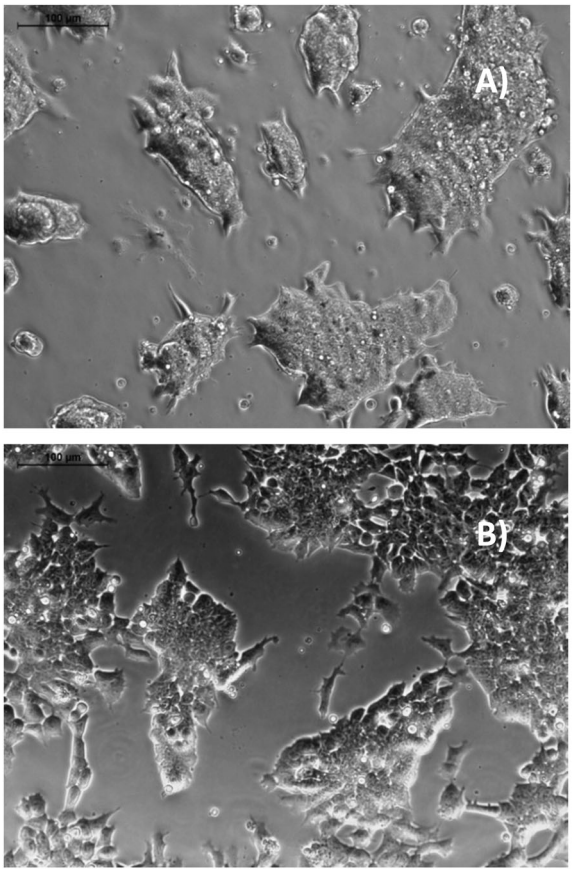

Fig. 8 Phase contrast image of ESC colonies two days after seeding on dishes coated with EUGL or gelatin. Stem cells grown on the EUGL film (upper image: A) and on a Petri gelatin-coated plate as a control (lower image: B). Scale bars: 100 μm.

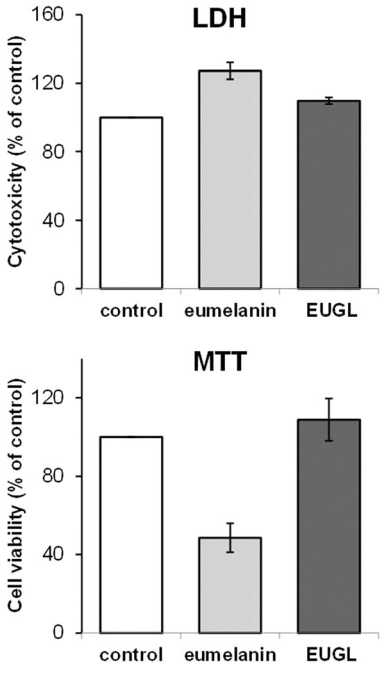

Fig. 9 Effects of melanin and EUGL on microglial cell membrane integrity (LDH) and on the microglial cell mitochondrial membrane function (MTT). Primary rat microglial cells were grown on eumelanin and EUGL for 24 h. The cytotoxicity was assessed respectively by lactate dehydrogenase (LDH) assays and by MTT reduction assay. Values are expressed as mean ± S.D (n = 4).

a cell typology of hematopoietic origin. Indeed it could be speculated that the different morphology and chemical nature of EUGL and eumelanin could have stimulated, in the latter case, phagocytic activity in these cells and, therefore, induced cell death. However, this hypothesis deserves further investigations, in particular in relation to the morphology of EUGL *vs.* that of eumelanin.

Given the poor adhesivity of GL film on substrates, the intrinsic biocompatibility and toxicity toward mammalian cells of neat GL layers cannot be evaluated under the same experimental conditions reported for EUGL.

Experimental

Materials

All commercially available reagents were used as received and all the solvents were of analytical grade. 5,6-Dihydroxindole (DHI) and 2-carboxy-5,6-dihydroxindole (DHICA) were prepared according to a reported procedure.[54] CB, N110 type (furnace CB), was obtained by Sid Richardson Carbon Co. CB is a monodispersion of chain-like aggregates of spherical primary particles with average diameters of 15–20 nm. The hydrodynamic diameter of the aggregates is 170 ± 10 nm and the surface area is 139 $m^2\ g^{-1}$ (BET method).

Details about the preparation of GL layers, DHI and DHICA are reported in the ESI† section.

EUGL preparation

GL layers aqueous suspension (1 mg mL^{-1}) was added to the DHI–DHICA 3 : 1 mixture dissolved in methanol by ultrasonic agitation (20 mg mL^{-1}). The suspension was kept for 10 min under agitation using a magnetic stirrer; pH was then adjusted to 8 by the addition of ammonia solution (28% in water) allowing indole autooxidation and polymerization. After 1 h the reaction was quenched by adding acetic acid (1 M) until pH 4 was established. A EUGL film was obtained by drop casting the suspension onto clean substrates (well plates for biological assays, quartz and mica plates). For bulk analyses the suspension was dried in an oven at 80 °C. After drying the hybrid was found to be insoluble in water.

Details about the analytical techniques used to characterize the materials and aboutthe *in vitro* tests are reported in the ESI† section.

Conclusions

In light of possible effective interfacing of two π-materials, namely eumelanin and GL layers, we speculated on the possibility of accessing a biocompatible substrate featuring typical eumelanin properties, including adhesion and water stability, but exhibiting improved electrical conductivity with respect to the natural pigment.

In situ eumelanin preparation allowed the entrapment of GL layers producing a hybrid material possessing promising properties in view of applications in bioelectronics.

A possible model representation of EUGL structure is reported in Fig. 10 depicting EUGL as eumelanin coated GL layers. This hypothesis arises from the known properties of eumelanin, chiefly adhesion and affinity toward aromatic systems,[18,55] and

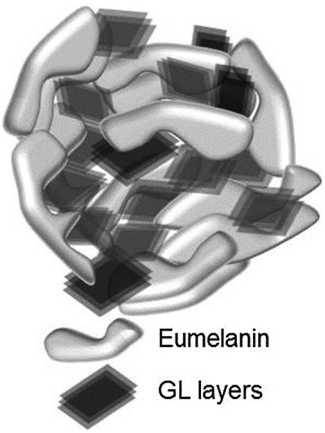

Fig. 10 Hypothesized morphologies of EUGL.

the observed adhesivity, mechanical stability to water and biocompatibility of EUGL. Indeed, given the water solubility of GL layers,[36] such EUGL features are ascribable to external exposition of eumelanin.

The wide biocompatibility of EUGL, capable of allowing ESC and MC culture, pairs with an unprecedented conductivity in a eumelanin derivative. EUGL exhibits an electrical conductivity more than 4 orders of magnitude greater than that of the parent eumelanin compound. It may be speculated that this conductivity increment with respect to eumelanin, besides the chemical nature of the EUGL has a contribution from the improved large scale homogeneity of the samples. This hypothesis would be supported by AFM images and associated with a better connection between uniformly distributed grains. In addition, the role of possible percolating paths of GL layers inside the compounds cannot be excluded (even if unlikely), and represents an issue deserving further investigation.

The properties of the EUGL films described herein may expand the scope of eumelanin in bioelectronics paving the way towards true biocompatible organic electrochemical transistor-like[56,57] interfaces capable of translating cellular activity into electrical signals.

Acknowledgements

This work was supported by a grant from Italian MIUR (PRIN 2010–2011, 010PFLRJR ''PROxi'' project), by a grant to SP from Ministry of University and Research for the projects: Futuro in Ricerca 2013 (RBFR13YZ2Y) and was carried out in the frame of the EuMelaNet program (http://www.espcr.org/eumelanet) and the PolyMed project within the FP7-PEOPLE-2013-IRSES frame, PIRSES-GA-2013-612538. The authors acknowledge the Accordo CNR-MSE ''Utilizzo pulito dei combustibili fossili ai fini del risparmio energetico'' 2011–2012 for the financial support.

Notes and references

1 J. Rivnay, R. M. Owens and G. G. Malliaras, *Chem. Mater.*, 2014, **26**, 679–685.
2 M. Berggren and A. Richter-Dahlfors, *Adv. Mater.*, 2007, **19**, 3201–3213.

3 M. d'Ischia, A. Napolitano, A. Pezzella, P. Meredith and T. Sarna, *Angew. Chem., Int. Ed.*, 2009, **48**, 3914–3921.
4 P. Meredith, C. J. Bettinger, M. Irimia-Vladu, A. B. Mostert and P. E. Schwenn, *Rep. Prog. Phys.*, 2013, **76**, 034501.
5 M. d'Ischia, K. Wakamatsu, A. Napolitano, S. Briganti, J. C. Garcia-Borron, D. Kovacs, P. Meredith, A. Pezzella, M. Picardo, T. Sarna, J. D. Simon and S. Ito, *Pigm. Cell Melanoma Res.*, 2013, **26**, 616–633.
6 C. Santato and F. Cicoira, *Organic Electronics Emerging Concepts and Technologies Preface*, Blackwell Science Publ, Oxford, 2013.
7 S. Ito, *Pigm. Cell Melanoma Res.*, 2009, **22**, 12–13.
8 S. Ito, *Melanins and Melanosomes: Biosynthesis, Biogenesis, Physiological, and Pathological Functions*, Wiley-VCH Verlag Gmbh, Pappelallee 3, W-69469 Weinheim, Germany, 2011.
9 L. Ascione, A. Pezzella, V. Ambrogi, C. Carfagna and M. d'Ischia, *Photochem. Photobiol.*, 2013, **89**, 314–318.
10 A. Pezzella, A. Iadonisi, S. Valerio, L. Panzella, A. Napolitano, M. Adinolfi and M. D'Ischia, *J. Am. Chem. Soc.*, 2009, **131**, 15270–15275.
11 A. Huijser, A. Pezzella and V. Sundstrom, *Phys. Chem. Chem. Phys.*, 2011, **13**, 9119–9127.
12 V. Capozzi, G. Perna, P. Carmone, A. Gallone, M. Lastella, E. Mezzenga, G. Quartucci, M. Ambrico, V. Augelli, P. F. Biagi, T. Ligonzo, A. Minafra, L. Schiavulli, M. Pallara and R. Cicero, *Thin Solid Films*, 2006, **511**, 362–366.
13 D. Rettenwander, P. Blaha, R. Laskowski, K. Schwarz, P. Bottke, M. Wilkening, C. A. Geiger and G. Amthauer, *Chem. Mater.*, 2014, **26**, 2617–2623.
14 J. Wünsche, Y. Deng, P. Kumar, E. Di Mauro, E. Josberger, J. Sayago, A. Pezzella, F. Soavi, F. Cicoira, M. Rolandi and C. Santato, *Chem. Mater.*, 2015, **27**, 436–442.
15 P. Meredith and T. Sarna, *Pigm. Cell Res.*, 2006, **19**, 572–594.
16 Y. Liu and J. D. Simon, *Pigm. Cell Res.*, 2005, **18**, 42–48.
17 S. Reale, M. Crucianelli, A. Pezzella, M. D'Ischia and F. De Angelis, *J. Mass Spectrom.*, 2012, **47**, 49–53.
18 M. Arzillo, G. Mangiapia, A. Pezzella, R. K. Heenan, A. Radulescu, L. Paduano and M. D'Ischia, *Biomacromolecules*, 2012, **13**, 2379–2390.
19 D. Kai, M. P. Prabhakaran, G. R. Jin and S. Ramakrishna, *J. Mater. Chem. B*, 2013, **1**, 2305–2314.
20 Q. L. Fan, K. Cheng, X. Hu, X. W. Ma, R. P. Zhang, M. Yang, X. M. Lu, L. Xing, W. Huang, S. S. Gambhir and Z. Cheng, *J. Am. Chem. Soc.*, 2014, **136**, 15185–15194.
21 A. Pezzella, M. Barra, A. Musto, A. Navarra, M. Alfe, P. Manini, S. Parisi, A. Cassinese, V. Criscuolo and M. d'Ischia, *Mater. Horiz.*, 2015, **2**, 212–220.
22 M. Muskovich and C. J. Bettinger, *Adv. Healthcare Mater.*, 2012, **1**, 248–266.
23 C. J. Bettinger, P. P. Bruggeman, A. Misra, J. T. Borenstein and R. Langer, *Biomaterials*, 2009, **30**, 3050–3057.
24 C. Kremer, C. Witte, S. L. Neale, J. Reboud, M. P. Barrett and J. M. Cooper, *Angew. Chem., Int. Ed.*, 2014, **53**, 842–846.
25 L. Y. Feng, L. Wu and X. G. Qu, *Adv. Mater.*, 2013, **25**, 168–186.
26 J. Wunsche, F. Cicoira, C. F. O. Graeff and C. Santato, *J. Mater. Chem. B*, 2013, **1**, 3836–3842.
27 J. Wunsche, L. Cardenas, F. Rosei, F. Cicoira, R. Gauvin, C. F. O. Graeff, S. Poulin, A. Pezzella and C. Santato, *Adv. Funct. Mater.*, 2013, **23**, 5591–5598.
28 F. Bloisi, A. Pezzella, M. Barra, F. Chiarella, A. Cassinese and L. Vicari, *J. Appl. Phys.*, 2011, **110**, 026105.
29 F. Bloisi, A. Pezzella, M. Barra, M. Alfe, F. Chiarella, A. Cassinese and L. Vicari, *Appl. Phys. A: Mater. Sci. Process.*, 2011, **105**, 619–627.
30 C. Pezzella, L. Guarino and A. Piscitelli, *Cell. Mol. Life Sci.*, 2015, **72**, 923–940.
31 X. W. Ou, P. L. Chen, L. Jiang, Y. F. Shen, W. P. Hu and M. H. Liu, *Adv. Funct. Mater.*, 2014, **24**, 543–554.
32 H. A. Becerril, R. M. Stoltenberg, M. L. Tang, M. E. Roberts, Z. F. Liu, Y. S. Chen, D. H. Kim, B. L. Lee, S. Lee and Z. A. Bao, *ACS Nano*, 2010, **4**, 6343–6352.
33 J. B. Wu, M. Agrawal, H. A. Becerril, Z. N. Bao, Z. F. Liu, Y. S. Chen and P. Peumans, *ACS Nano*, 2010, **4**, 43–48.
34 J. Kim, L. J. Cote and J. X. Huang, *Acc. Chem. Res.*, 2012, **45**, 1356–1364.
35 X. Wang, L. J. Zhi and K. Mullen, *Nano Lett.*, 2008, **8**, 323–327.
36 M. Alfe, V. Gargiulo, R. Di Capua, F. Chiarella, J. N. Rouzaud, A. Vergara and A. Ciajolo, *ACS Appl. Mater. Interfaces*, 2012, **4**, 4491–4498.
37 M. Alfe, V. Gargiulo, L. Lisi and R. Di Capua, *Mater. Chem. Phys.*, 2014, **147**, 744–750.
38 E. Carella, M. Ghiazza, M. Alfè, E. Gazzano, D. Ghigo, V. Gargiulo, A. Ciajolo, B. Fubini and I. Fenoglio, *BioNanoSci.*, 2013, **3**, 112–122.
39 S. Stankovich, R. D. Piner, S. T. Nguyen and R. S. Ruoff, *Carbon*, 2006, **44**, 3342–3347.
40 M. D'Ischia, K. Wakamatsu, A. Napolitano, S. Briganti, J. C. Garcia-Borron, D. Kovacs, P. Meredith, A. Pezzella, M. Picardo, T. Sarna, J. D. Simon and S. Ito, *Pigm. Cell Melanoma Res.*, 2013, **26**, 616–633.
41 F. Zhang, X. Chen, R. A. Boulos, F. Md Yasin, H. Lu, C. Raston and H. Zhang, *Chem. Commun.*, 2013, **49**, 4845–4847.
42 F. De Marchi, D. Cui, J. Lipton-Duffin, C. Santato, J. M. MacLeod and F. Rosei, *J. Chem. Phys.*, 2015, **142**, 101923.
43 M. M. Jastrzebska, H. Isotalo, J. Paloheimo and H. Stubb, *J. Biomater. Sci., Polym. Ed.*, 1995, **7**, 577–586.
44 W. Osak, K. Tkacz, J. Slawinski and H. Czternastek, *Biopolymers*, 1989, **28**, 1875–1883.
45 L. Glasser and R. L. Fiederlein, *Am. J. Clin. Pathol.*, 1979, **72**, 956–962.
46 L. J. van der Pauw, *Philips Res. Rep.*, 1973, **28**, 158–178.
47 S. R. Cicco, M. Ambrico, P. F. Ambrico, M. M. Talamo, A. Cardone, T. Ligonzo, R. Di Mundo, C. Giannini, T. Sibillano, G. M. Farinola, P. Manini, A. Napolitano, V. Criscuolo and M. D'Ischia, *J. Mater. Chem. C*, 2015, **3**, 2810–2816.
48 M. R. S. Abouzari, F. Berkemeier, G. Schmitz and D. Wilmer, *Solid State Ionics*, 2009, **180**, 922–927.
49 E. Casero, A. M. Parra-Alfambra, M. D. Petit-Dominguez, F. Pariente, E. Lorenzo and C. Alonso, *Electrochem. Commun.*, 2012, **20**, 63–66.
50 I. N. Wang, J. T. Robinson, G. Do, G. Hong, D. R. Gould, H. Dai and P. C. Yang, *Small*, 2014, **10**, 1479–1484.

51 M. L. Block, L. Zecca and J. S. Hong, *Nat. Rev. Neurosci.*, 2007, **8**, 57–69.
52 S. M. Hussain and J. M. Frazier, *Toxicol. Sci.*, 2002, **69**, 424–432.
53 J. Carmichael, W. G. DeGraff, A. F. Gazdar, J. D. Minna and J. B. Mitchell, *Cancer Res.*, 1987, **47**, 943–946.
54 R. Edge, M. D'Ischia, E. J. Land, A. Napolitano, S. Navaratnam, L. Panzella, A. Pezzella, C. A. Ramsden and P. A. Riley, *Pigm. Cell Res.*, 2006, **19**, 443–450.
55 T. Sarna and H. A. Swartz, *The Pigmentary System: Physiology and Pathophysiology*, 2nd edn, 2007, pp. 311–341.
56 M. Bongo, O. Winther-Jensen, S. Himmelberger, X. Strakosas, M. Ramuz, A. Hama, E. Stavrinidou, G. G. Malliaras, A. Salleo, B. Winther-Jensen and R. M. Owens, *J. Mater. Chem. B*, 2013, **1**, 3860–3867.
57 D. Khodagholy, J. Rivnay, M. Sessolo, M. Gurfinkel, P. Leleux, L. H. Jimison, E. Stavrinidou, T. Herve, S. Sanaur, R. M. Owens and G. G. Malliaras, *Nat. Commun.*, 2013, **4**, 2133.